



**HAL**  
open science

# MODELLING OF POLYCRYSTALS USING WELL-CONTROLLED VORONOI-TYPE TESSELLATIONS AND ITS APPLICATIONS TO MICROMECHANICAL ANALYSES

Baptiste Flipon, L Milhem, Clément Keller, Romain Quey, Fabrice Barbe

► **To cite this version:**

Baptiste Flipon, L Milhem, Clément Keller, Romain Quey, Fabrice Barbe. MODELLING OF POLYCRYSTALS USING WELL-CONTROLLED VORONOI-TYPE TESSELLATIONS AND ITS APPLICATIONS TO MICROMECHANICAL ANALYSES. F. Willot and S. Forest Eds. International Workshop on the Physics and Mechanics of Random Structures: from Morphology to Material Properties, Presse des Mines, 2018, 978-2-35671-529-6. hal-01916848

**HAL Id: hal-01916848**

**<https://normandie-univ.hal.science/hal-01916848>**

Submitted on 8 Nov 2018

**HAL** is a multi-disciplinary open access archive for the deposit and dissemination of scientific research documents, whether they are published or not. The documents may come from teaching and research institutions in France or abroad, or from public or private research centers.

L'archive ouverte pluridisciplinaire **HAL**, est destinée au dépôt et à la diffusion de documents scientifiques de niveau recherche, publiés ou non, émanant des établissements d'enseignement et de recherche français ou étrangers, des laboratoires publics ou privés.

## **MODELLING OF POLYCRYSTALS USING WELL-CONTROLLED VORONOI-TYPE TESSELLATIONS AND ITS APPLICATIONS TO MICROMECHANICAL ANALYSES**

B. Flipon<sup>a</sup>, L. Milhem<sup>a,b</sup>, C. Keller<sup>a</sup>, R. Quey<sup>c</sup>, F. Barbe<sup>a</sup>

<sup>a</sup> Normandie Univ, INSA Rouen, UNIROUEN, CNRS, GPM, 76000 Rouen, France,

baptiste.flipon@insa-rouen.fr, luc.milhem@insa-rouen.fr, clement.keller@insa-rouen.fr, fabrice.barbe@insa-rouen.fr;

<sup>b</sup> FAVI S.A. – 14 rue Louis Deneux, 80490 Hallencourt, France;

<sup>c</sup> Univ. Lyon, IMT Mines Saint-Etienne, Centre SMS, CNRS, LGF, 42023 Saint-Etienne, France,

romain.quey@mines-stetienne.fr

This paper provides a review of our developments on the use of Voronoi-type tessellations for the analysis of the deformation of polycrystalline structures. This work was initiated 20 years ago by a fruitful collaboration with Dominique Jeulin and is still guided by his works. We introduce different types of tessellations and explain how they can be used by presenting several micromechanics cases of study, from the most simple to the most complex configurations.

**Keywords:** Polycrystals, Voronoi tessellation, Laguerre tessellation, Johnson-Mehl tessellation, Micromechanics

### **1 Introduction**

The mechanisms governing the elasto-plastic deformation, damage and fracture of metallic alloys are intimately related to their polycrystalline microstructures. This has motivated since the 90s the development of full-field modelling approaches to predict their behaviors. In the simulations, polycrystals are usually represented as Voronoi tessellations generated from a uniform random distribution of seed points, so-called “Poisson-Voronoi tessellations” [1]. However, Poisson-Voronoi tessellations are, at best, only partly representative of experimental microstructures. This is especially the case for microstructures optimized to enhance their mechanical properties, which may contain columnar or elongated grains (arising from solidification or forming operations, respectively), grain-size gradients, wide or even bimodal grain size distributions, etc.

In this paper, we present the series of developments on the modelling and micromechanics of complex experimental microstructures that we have carried out since our years spent with Dominique Jeulin, and that have been implemented in the specialized free (open-source) Neper software package [18, 19]. First, we show how particular choices in the spatial distribution of the seed points of a Voronoi tessellation can lead to well-controlled size-gradient structures of mixed equiaxed/columnar structures. Then, we introduce Laguerre tessellations (a generalization of the Voronoi algorithm to weighted tessellations) and demonstrate how they can be used to represent experimental microstructures described by multiple metrics, using optimization. Finally, we present Johnson-Mehl tessellations (a generalization of Voronoi tessellations to time-dependent nucleation and growth rates) and show how they can be used in the context of diffusive transformations of polycrystals. These developments are illustrated by specific cases of study on the micromechanics of polycrystals, which have been further addressed with finite element analyses. These developments not only lead to high-end tools for the modelling of existing materials but are also meant to provide a complementary, “numerical” strategy in material engineering approaches related to new manufacturing capabilities.

### **2 Voronoi tessellations**

#### **2.1 Definition**

Let us define  $D$  as a domain of space and  $G_i$  as a set of points distributed in  $D$ , defined by their coordinates. A Voronoi cell  $C_i$  is associated to each seed point ( $G_i$ ) as follows:

$$C_i = \{P(\underline{x}) \in D \mid d(P, G_i) < d(P, G_j) \ \forall j \neq i\}, \quad (1)$$

where  $d(A, B)$  corresponds to the Euclidean distance between  $A$  and  $B$ . Figure 1, which is taken from the seminal work of Dominique Jeulin and applied in Ref. [1], illustrates the construction of a Voronoi tessellation in 2D. Typically, the seed points are distributed randomly according to a uniform distribution, which leads

to so-called “Poisson-Voronoi tessellations”. Poisson-Voronoi tessellations are composed of convex cells of random sizes and shapes, and so are good first-order approximations of real polycrystals and are relatively easy to mesh into finite elements [18]. This is why they have become a standard in polycrystal computations of elastoplastic deformation [2, 23], fatigue [8], intergranular fracture [4], cleavage fracture [15], etc. A review of such applications to the full-field modelling of polycrystals is provided in [5], and an extensive list of the works carried out with Neper (most of which using Voronoi tessellations) can be found on the Neper website [17] (125 papers as of March 2018).

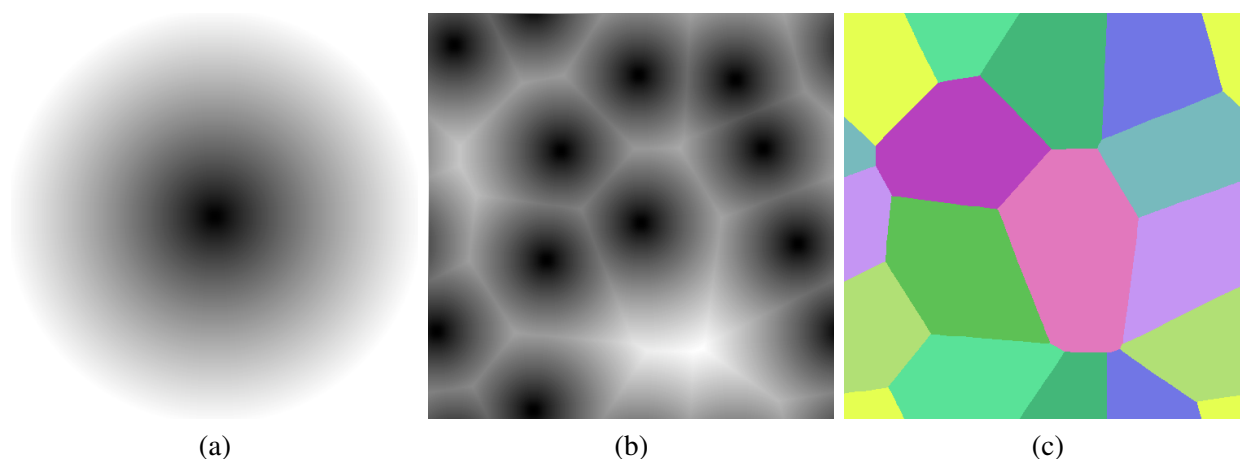


Figure 1: Construction of a Voronoi tessellation on a periodic grid [1]. (a) Distance function of a single seed point, (b) distance function of a set of seed points and (c) final result after cell construction and labelling.

## 2.2 Application to size-gradient structures

Introducing a grain size gradient in a polycrystalline material, with smaller grains near the surface, can improve its resistance to fatigue [20]. Such a microstructure can be represented by a Voronoi tessellation relatively simply: as the size of a cell is directly related to the distance between its seed and the surrounding seeds, a gradient of volume density of the seeds (in the domain) results in a gradient of size of the corresponding cells. In practice, the seeds can first be distributed on a regular array, where the distance between seeds is determined from the expected density at that location of the domain, and then slightly shifted about their nominal positions to retrieve random morphologies. The advantage of this method is twofold, as it controls the global size gradient as well as the minimum and maximum cell sizes. However, these properties are quite sensitive to the parameters of the seed distribution, so that they must be defined with great care. This is illustrated on Figure 2, where the complex interdependencies between the setting of the nominal regular array of seeds and the prescribed range of the perturbation distance lead to 2D microstructures with grain shapes and size gradient that are not representative of real materials. To better understand (and monitor) these interdependencies, a procedure based on an objective and reproducible construction of the inputs has been developed to explore the types of microstructures that can be obtained from a unidirectional gradient in a 2D domain: all the inputs have been defined in terms of a limited number of parameterized equations and the parameters space has been fully explored automatically. This enabled us to identify suitable values for the spacings between seeds and the perturbations distances that could then be used for the 3D tessellations. Figure 3 presents two examples of such microstructures, with low and high gradients, respectively.

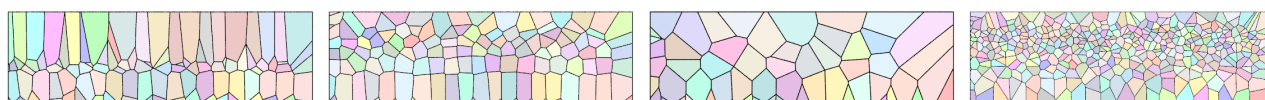


Figure 2: Examples of some remarkable 2D size-gradient tessellations extracted from the exploration of the parameters space used to define the inputs of the tessellation.

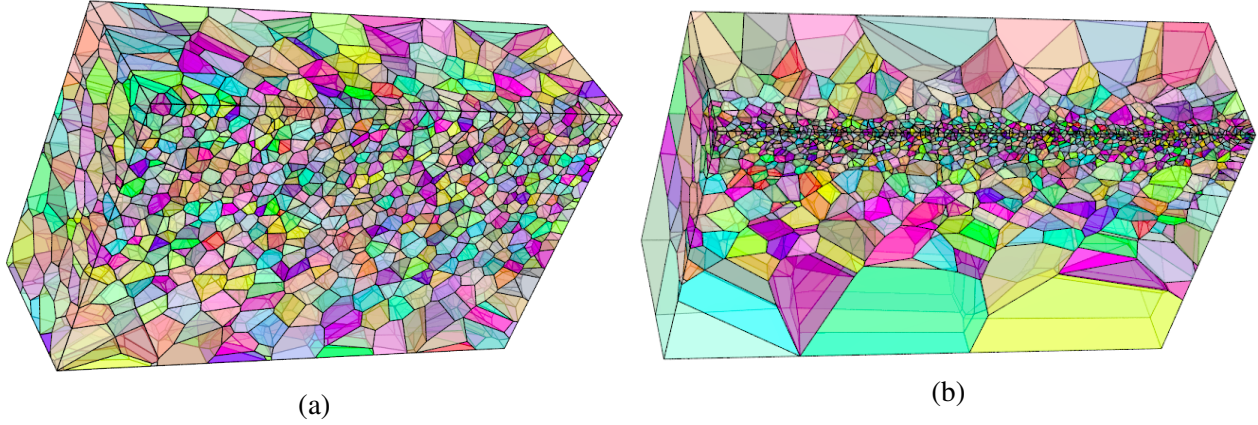


Figure 3: Examples of two 3D size-gradient tessellations, with (a) low and (b) high size gradients.

### 2.3 Application to mixed equiaxed/columnar structures

Columnar grains can be obtained by directional solidification and are desirable in some applications, *e.g.* in turbine blades, to avoid the existence of grain boundaries perpendicular to the radial direction, which is subjected to high centrifugal forces. During elaboration, columnar grains usually appear near the outer surface of die-cast parts, as a result of very fast solidification and high temperature gradients. In this case, columnar grains generally coexist with equiaxed grains, which are located at the center, as illustrated on Fig. 4a. Equiaxed grains have random (crystallographic) orientations whereas columnar grains have orientations characterized by a crystallographic direction (typically  $\langle 100 \rangle$  for cubic metals) parallel to the solidification direction, giving rise to an intense fibre texture. The deformation of such microstructures can only be predicted by full-field modelling, as they show grain morphologies and crystallographic orientation distributions distinctly different of those of “conventional” microstructures. This type of structures can be represented by Voronoi tessellations, by distributing the seeds as illustrated on Fig. 4. As for their deformation, we showed in Ref. [7] that the crystallographic texture of the columnar grains drives their own plastic deformation but also the stress distribution of the equiaxed grains (Fig. 5).

## 3 Laguerre tessellations

### 3.1 Definition

Similarly to Voronoi tessellations, Laguerre tessellations are generated from seed points ( $G_i$ ) of given coordinates, but these seed points are attributed weights,  $w_i$ . A laguerre cell is associated to each seed point as follows:

$$C_i = \{P(\underline{x}) \in D \mid d(P, G_i)^2 - w_i < d(P, G_j)^2 - w_j \quad \forall j \neq i\} \quad (2)$$

The higher the weight of a seed, the larger its associated cell. A Voronoi tessellation is obtained if all weights are equal. Figure 6 illustrates the construction of a Laguerre tessellation in 2D. Laguerre tessellations are more general than Voronoi tessellations, as they can reproduce any tessellation composed of convex cells [13]. However, not only the seed positions but also the seed weights need to be properly controlled, which is not trivial. Still, it can be clearly seen from Fig. 6 that Laguerre tessellations can include wider grain size distributions than Voronoi tessellations. Most of the applications of Laguerre tessellations concern the modelling of microstructures of polycrystals or foams [14, 12], while their applications to mechanical or physical analyses are much more rare.

### 3.2 Application to bimodal grain size distributions

Grain size refinement is known to improve the yield stress of metallic alloys but also to degrade their ductility, which can be detrimental for material forming. Several approaches have been developed to evade this strength-ductility dilemma. One of the most promising approach consists in architecturing the microstructure in phases of

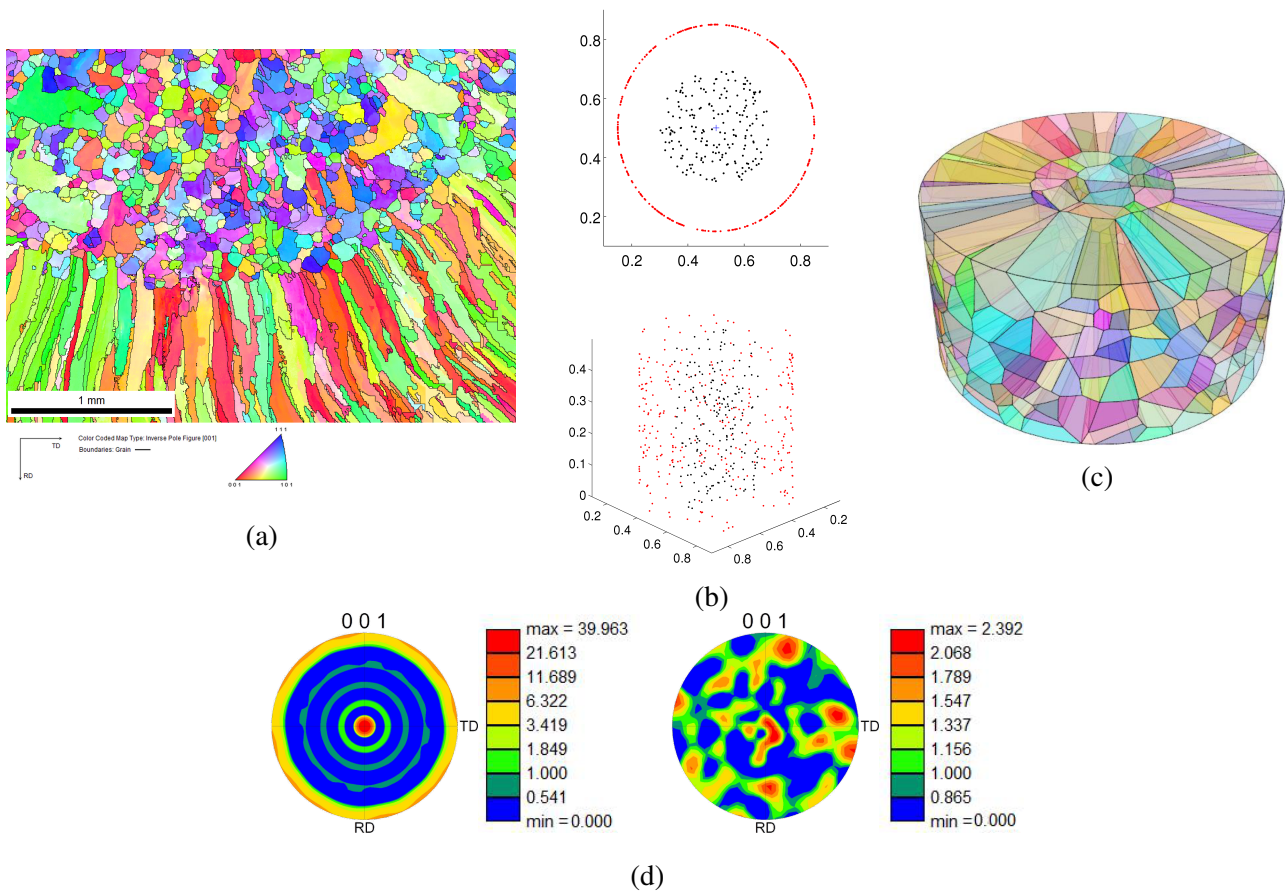


Figure 4: Mixed equiaxed/columnar structure: (a) Orientation map (inverse pole figure) of the section of a die-cast cylinder including both equiaxed grains and columnar grains. (b) Distribution of seed points, where the black points generate equiaxed cells and the red points generate columnar cells, seen as top and perspective views, (c) resulting Voronoi tessellation and (d) orientation distributions of the (left) columnar and (right) equiaxed grains, shown as  $\langle 100 \rangle$  pole figures.

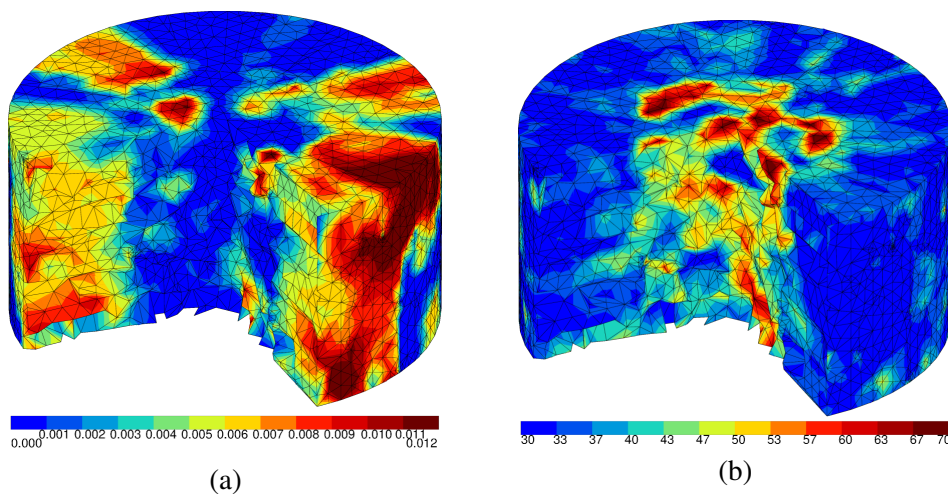


Figure 5: Crystal plasticity finite element simulation of the tensile deformation of the cylinder with mixed equiaxed/columnar grains: (a) plastic strain field and (b) von Mises stress field.

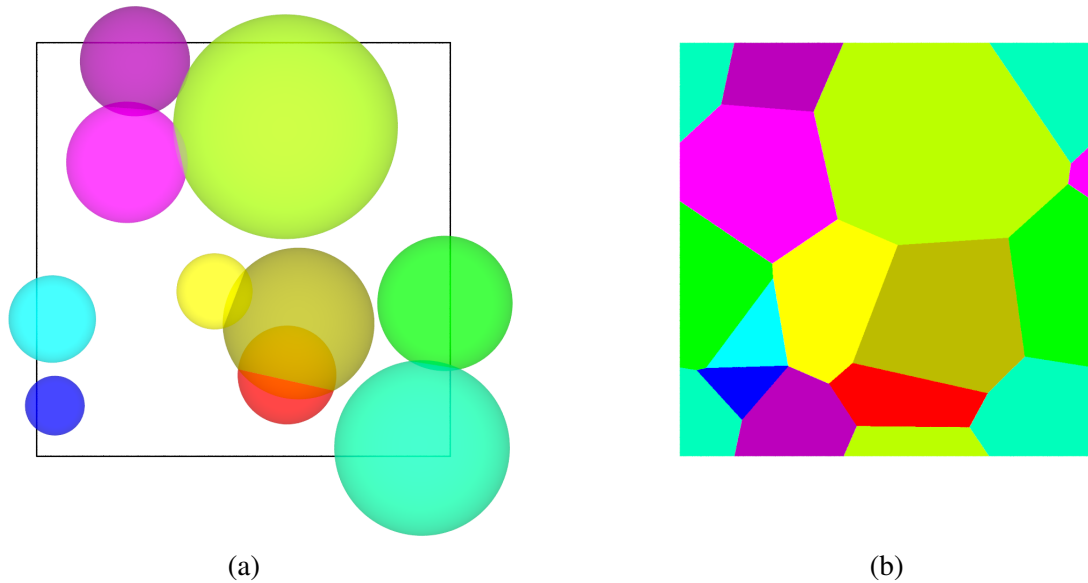


Figure 6: Construction of a periodic Laguerre tessellation. (a) Seeds represented as spheres of centre  $G_i$  and radius  $\sqrt{w_i}$ , and (b) corresponding cells.

different properties, which has lead, in particular, to the concept of bimodal polycrystals, for which ultrafine grains coexist with coarse grains. Such polycrystals have been elaborated by means of powder metallurgy and spark plasma sintering and, as shown in Fig. 7, exhibit properties significantly different of those of “conventional” materials [6, 7]. These results then rise questions on the optimization of such bimodal materials: what should be the volume fractions of the two grain populations? and how should these populations be spatially distributed? Full-field modelling provides efficient means to address these questions. Preliminary analyses have dealt with the representativeness of the considered volume element as regards its effective properties. It has been shown that a single coarse grain embedded in a matrix of ultrafine grains (Fig. 8a-b) is not convenient, and that the grain size distribution alone is not sufficient to describe the microstructure: the spatial arrangement of the coarse grains can play a significant role, as shown on Fig. 8c and 9.

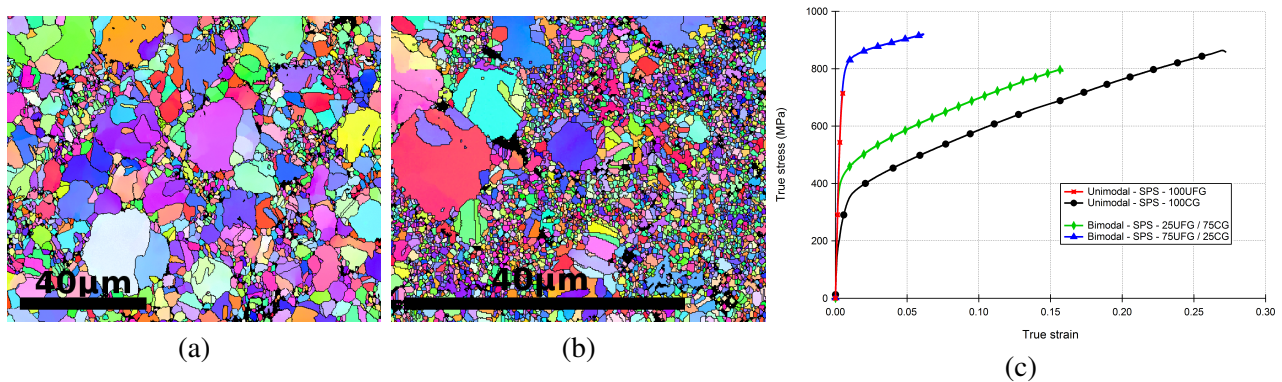


Figure 7: EBSD maps of bimodal 316L steel polycrystals elaborated by spark plasma sintering: (a) 75%  $15\mu\text{m}$ -coarse-grains, 25%  $0.5\mu\text{m}$ -fine-grains, (b) 25%  $15\mu\text{m}$ -coarse-grains, 75%  $0.5\mu\text{m}$ -fine-grains, (c) tensile responses of unimodal and bimodal 316L steel specimens elaborated by spark plasma sintering. After [6].

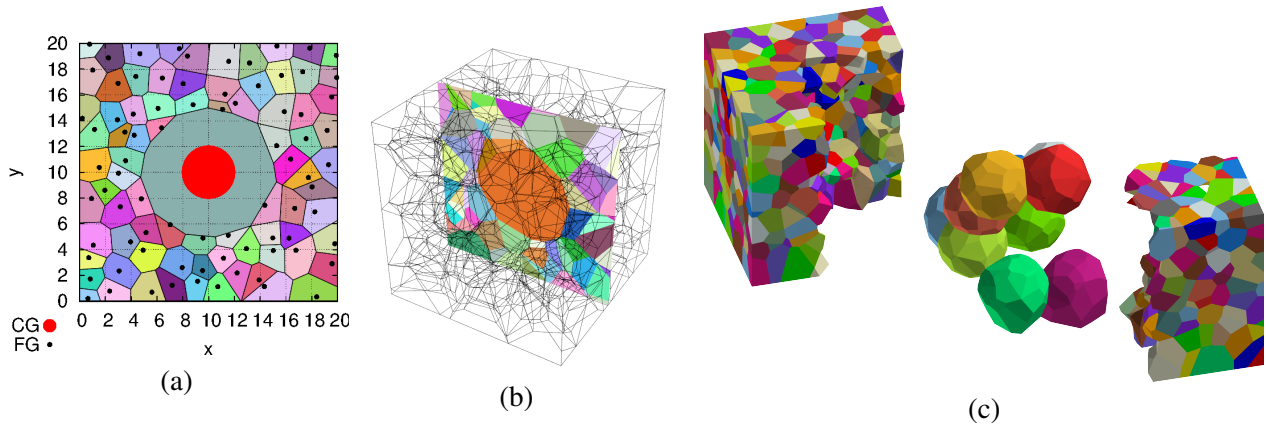


Figure 8: Generation of a polycrystal with coarse grains embedded in a matrix of fine grains: (a) positions and weights of the seeds for a 2D generation and the resulting cells, (b) extension of (a) in 3D, (c) extension of (b) for a cluster of coarse grains.

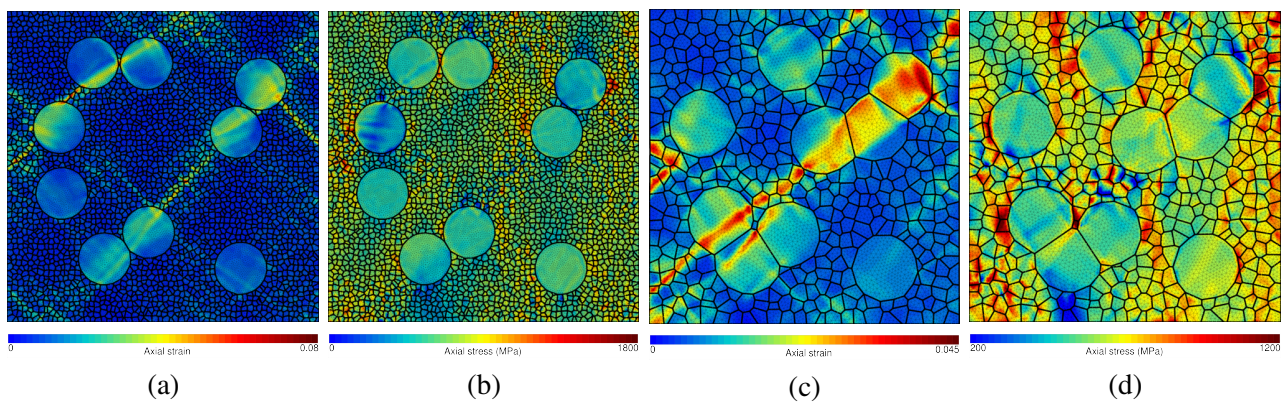


Figure 9: Stress and strain fields for two realizations of microstructures: (a-b) isolated coarse grains, (c-d) clustered coarse grains. As a pragmatic approach, a Hall-Petch term has been introduced in the definition of the resolved shear stress hardening rule to account for grain size effect.

### 3.3 Application to specified grain size and sphericity distributions

When several grain properties must be controlled, it becomes extremely difficult to determine the seeds positions and weights of a Laguerre tessellation *a priori*, as was done previously. We then employ an optimization approach [19], for which the variables are the seed positions and weights and the objective function ( $\mathcal{O}$ , to minimize) quantifies the difference between the target and current cell properties,

$$\mathcal{O} = \sqrt{\frac{1}{n} \sum_{s=1}^n \mathcal{A}^{s2}}, \quad (3)$$

where each of the  $\mathcal{A}^s$  concern a particular property. As mentioned before, the properties can describe the morphology and arrangement of the grains, *i.e.* their sizes, shapes, positions, etc. Experimentally, grain properties such as their sizes or shapes are generally described by their distributions. To define  $\mathcal{A}$ , it is then needed to compare the set of (discrete) cell values to a (continuous) target distribution. This is a well-known problem in experimental physics (or medicine), for which different metrics (or “tests”) have been proposed from 1930–1970. We employ a test of the form

$$\mathcal{A}^s = \int_{-\infty}^{+\infty} \frac{[X^s(x) - F^s(x)]^2}{F^s(x) [1 - F^s(x)]} dx \quad \text{with} \quad \begin{cases} F^s = F \circ s \\ X^s = X \circ s \end{cases} \quad (4)$$

where  $F$  represents the target cumulative distribution function,  $X$  represents the current cumulative distribution function, and  $s$  is a Gaussian smoothing kernel (used to facilitate optimization convergence).  $\mathcal{A}^s$  decreases as  $X^s$  converges to  $F^s$  and is equal to 0 when  $X^s = F^s$ . Figure 10 provides tessellations generated from different size and sphericity distributions. As microstructures with different properties can be generated automatically, it becomes easy to analyse microstructure-property relationships. Recent applications concern the simulation of thermal transport in nanocrystalline MoS<sub>2</sub> sheets, which is important in energy storage and microelectronics applications [21, 22]. The aim is to reduce the thermal diffusion of the material by counterbalancing the very fast diffusion in the crystalline structure by the high density of grain boundaries (of slower diffusion) of a nanocrystalline structure. The macroscopic thermal conductivity therefore depends on the average grain size, but it may also depend on the grain size distribution. This is illustrated on Fig. 11 in the case of nanocrystalline graphene. Note how wider grain size distributions result in higher conductivities due to the presence of preferential diffusion paths.

## 4 Johnson-Mehl tessellations

### 4.1 Definition

The Johnson-Mehl tessellation is obtained by combining nucleation (through a sequential intensity  $\dot{N}(t)$ ) and growth (with growth rate  $\alpha(t)$ ) [10]. Considering the sequence of seed points  $G_i(\underline{x}_i, t_i)$ , a cell  $C_i$  is associated to each seed point ( $G_i$ ) as follows:

$$C_i = \left\{ P(\underline{x}) \in D \mid d(P, G_i(\underline{x}_i, t_i)) - \alpha(t_i) t_i < d(P, G_j(\underline{x}_j, t_j)) - \alpha(t_j) t_j \quad \forall j \neq i \right\}, \quad (5)$$

The nucleation ( $\dot{N}(t)$ ) and growth ( $\alpha(t)$ ) laws can be arbitrary, so that Johnson-Mehl tessellations are more general than Voronoi tessellations and can include non-convex cells. Figure 12 ( $v_f = 1$ ) provides an example of a Johnson-Mehl tessellation. A Voronoi tessellation is obtained if all seed points nucleate at the same time and growth is isotropic. When a Johnson-Mehl tessellation is constructed in the context of phase transformation, the nucleation ( $\dot{N}(t)$ ) and growth ( $\alpha(t)$ ) laws can be based on physical principles. Moreover, the transformation kinetics can then be described by the theory of Kolmogorov (1938), Johnson-Mehl (1939) and Avrami (1939), which is well-known for providing a simple and general law to describe the kinetics of formation of a product phase during a process of nucleation and growth. It takes the form  $v_f(t) = 1 - \exp(-kt^n)$  where  $v_f$  is the product phase volume fraction and ( $k, n$ ) are parameters. This form generalizes the particular configuration of an isotropic growth at a constant velocity  $\alpha$  which had been considered by Johnson and Mehl: with this condition and in two particular cases of nucleation, the variation  $dv_f$  within a time interval  $dt$  can be integrated and the following evolution laws are obtained:

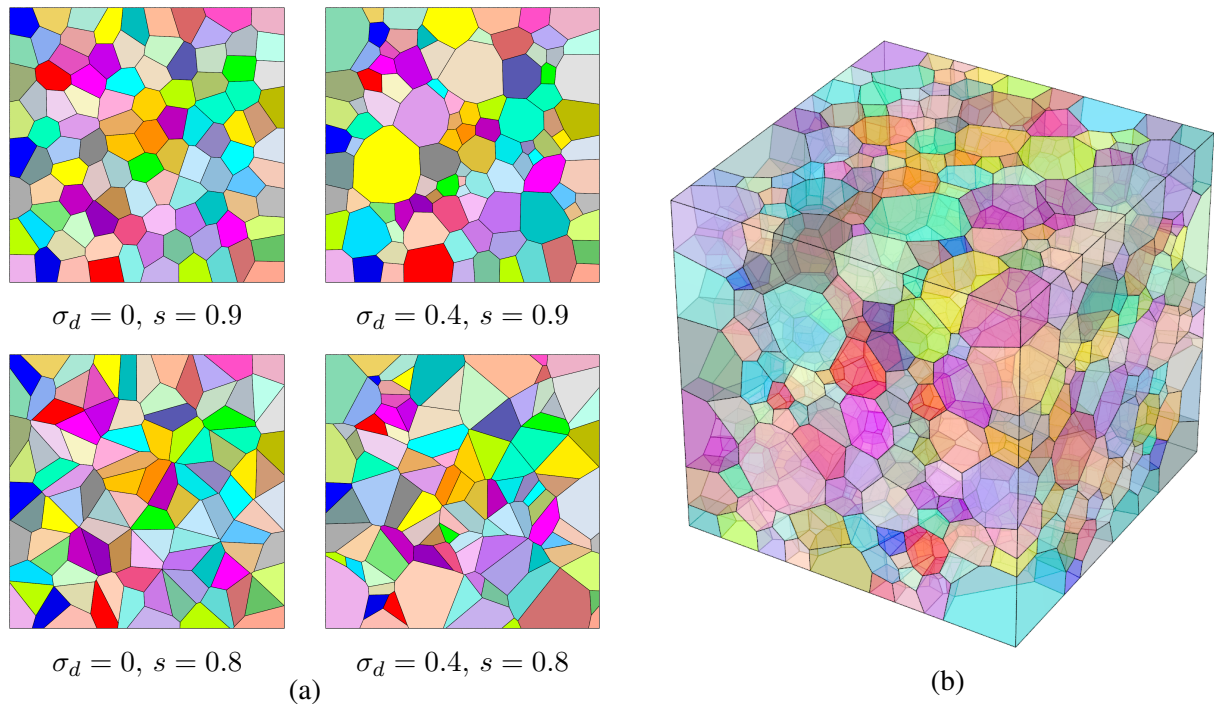


Figure 10: Tessellations generated from grain size and sphericity distributions. The normalized grain size distribution is a normal distribution of average 1 and standard deviation  $\sigma_d$ . The sphericity distribution is a normal distribution of average  $s$  and standard deviation 0.03. (a) 2D tessellations of different values of  $\sigma_d$  and  $s$  (100 cells). (a) 3D tessellations corresponding to a grain-growth polycrystal:  $\sigma_d = 0.35, s = 0.855$  (1000 cells).

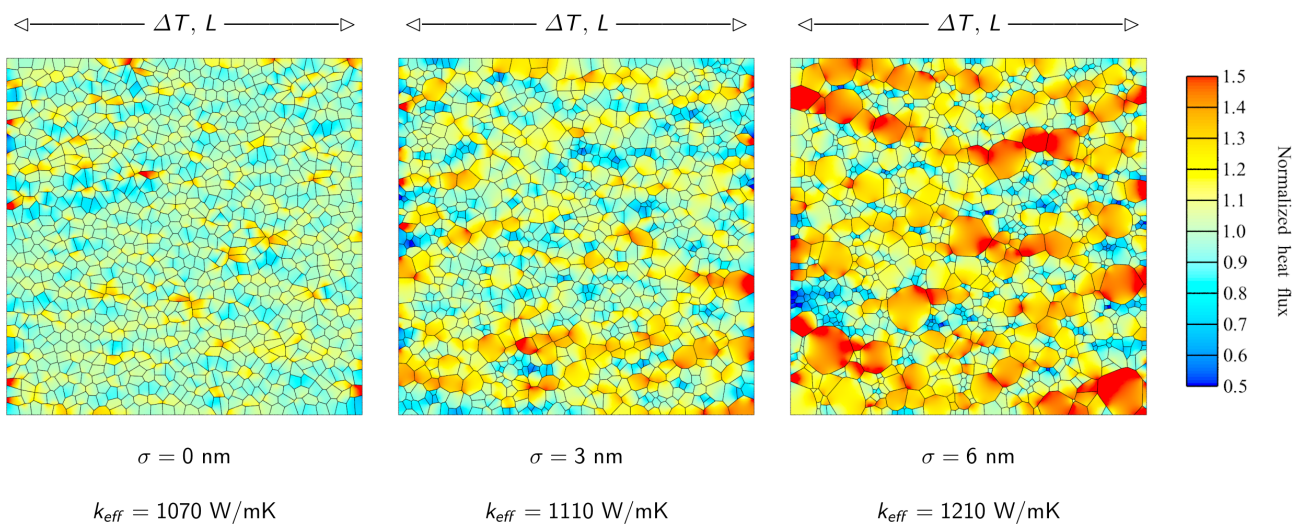


Figure 11: Thermal transport in nanocrystalline graphene sheets with the same average grain size ( $10 \mu\text{m}$ ) but different grain size distributions.

- for a simultaneous nucleation with a density  $N_0$ :  $v_f(t) = 1 - \exp\left(-\frac{4\pi}{3} \alpha^3 N_0 t^3\right)$ ;
- for a constant nucleation rate  $\dot{N}$ :  $v_f(t) = 1 - \exp\left(-\frac{\pi}{3} \alpha^3 \dot{N} t^4\right)$ .

In the following, we will only consider the case of a constant growth rate.

## 4.2 Application to solid-solid phase transformations

The formation of Johnson-Mehl tessellations has been implemented in Neper and applied in Ref. [3] to describe the microstructure evolution of a polycrystal during a diffusive transformation. The general objective of the modelling is to account for the local elastoplastic interactions between grains of either the parent or the product phase to predict the residual stresses and the effective plasticity that are induced by a diffusive solid-solid phase transformation in a steel. The parent microstructure is a Voronoi tessellation which represents the austenitic (or ferritic) microstructure, and from which favourable nucleation sites of the product phase can be defined: grain corners, edges and surfaces, in decreasing order of likelihood. In Fig. 12, the nucleation sites are restricted to grain corners, and a constant growth velocity is considered. It can be seen how the resulting microstructure differs from a Voronoi tessellation, as grains are non convex. Fig. 13 illustrates the elastoplastic interactions that arise between grains during phase transformation, without any external loading (each grain has a crystal plasticity constitutive behavior corresponding to its phase). It appears that residual stresses and microplasticity are generated locally, which eventually influences the effective properties of the parent phase.

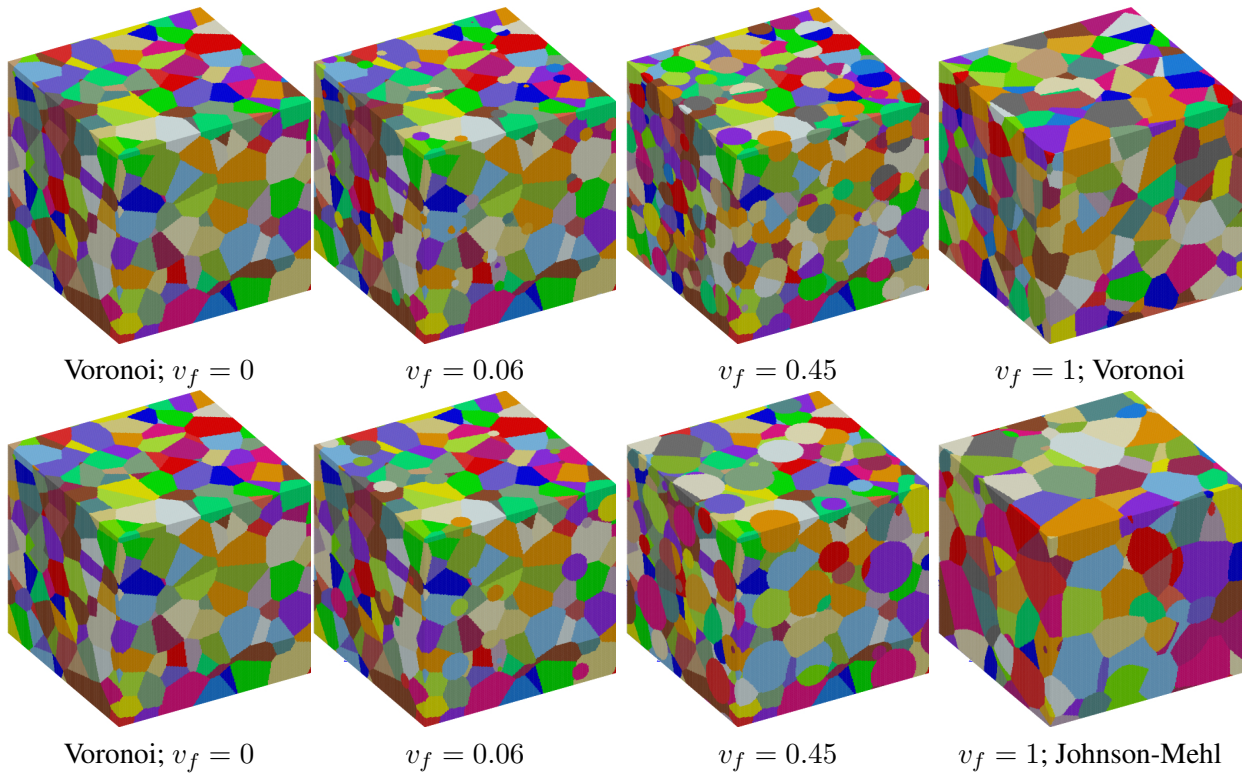


Figure 12: Two polycrystal-to-polycrystal microstructure evolutions corresponding to diffusive transformations at a constant growth velocity starting from the same Voronoi polycrystal. (Top) The nucleation is simultaneous with a given density  $N_0$  and Voronoi polyhedra are obtained. (Bottom) Nucleation takes place at a constant rate  $\dot{N}$  through time and non convex polyhedra are obtained. Each example is a particular case of a Johnson-Mehl tessellation. After [3].

## 5 Conclusion

In this paper, we provided an overview of the work we carried out as a continuation of our years spent with Dominique Jeulin. Dominique's playground, morphological mathematics, as well as his own contributions, have

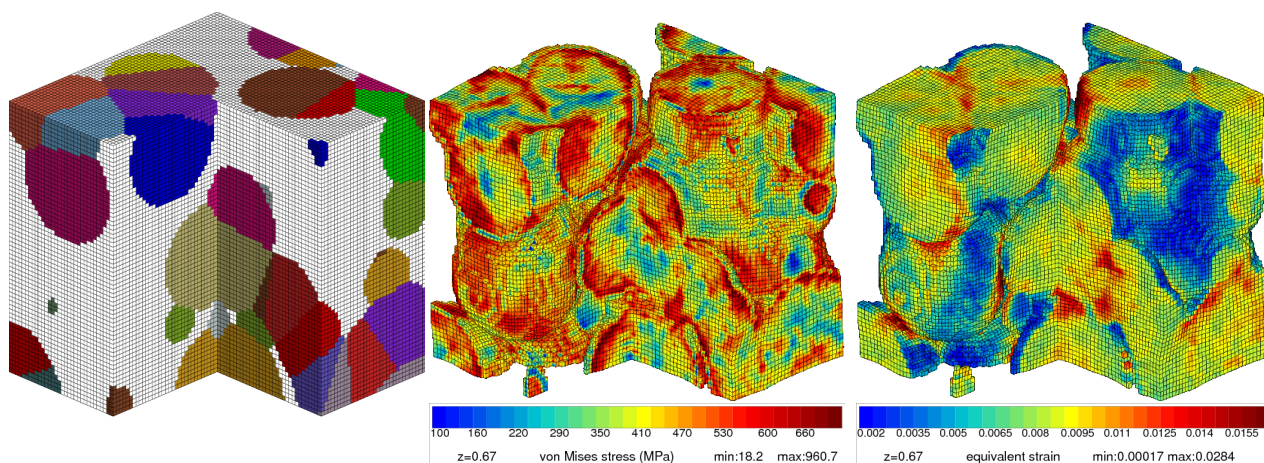


Figure 13: Stress-free transformation of a 85-grain austenite polycrystal to a 177-grain ferrite polycrystal. Volume fraction of ferrite is  $z = 0.67$ . (a) Grains of ferrite (parent austenitic grains are not represented). (b) Von Mises equivalent stress field on the contour of ferrite grains. (c) Equivalent total strain field on the contour of ferrite grains. A quarter of the polycrystal has been removed for visualisation sake. After [3].

of course been very important. We have developed several new strategies for representing random polycrystals by geometrical models and used the models in various applications. This approach is based on two main motivations:

- to reproduce existing materials with information on the microstructure which is as close to reality as possible;
- to generate polycrystals in a process of material engineering, *i.e.* to guide the development of architected materials and their elaboration by new processing technologies.

In both cases, the grain size distribution is an important property, but we have shown that it cannot be considered alone to accurately describe polycrystalline microstructures. Indeed, it is also necessary to control (at least) the grain shape [19]. Laguerre tessellations offer full control on these properties, and we have presented an optimization approach that exploits them to their full potential. Johnson-Mehl tessellations offer a more general formulation and are attractive in the context of phase transformations. >From a general point of view, on top of statistics, 2-point statistics are of course needed to characterize and control properties such as the percolation of large grains: in a polycrystal containing two distinctly different grain size populations, then, as shown in [7], the spatial distribution of the coarse grains (whether they are isolated or clustered for example) can have a significant effect on the effective behaviour. Once again, Dominique's contributions to the control of phase distributions in a morphological model [11, 9] or to the estimation of tortuosity in 3D [16] will be our sources of knowledge and knowhow.

## References

- [1] F. Barbe, L. Decker, D. Jeulin, and G. Cailletaud. Intergranular and intragranular behavior of polycrystalline aggregates. Part 1: F.E. model. *International Journal of Plasticity*, 17:513–536, 2001.
- [2] F. Barbe, S. Forest, and G. Cailletaud. Intergranular and intragranular behavior of polycrystalline aggregates. Part 2: results. *International Journal of Plasticity*, 17:537–563, 2001.
- [3] F. Barbe and R. Quey. A numerical modelling of 3D polycrystal-to-polycrystal diffusive phase transformations involving crystal plasticity. *International Journal of Plasticity*, 27:823–840, 2011.
- [4] I. Benedetti and M. Aliabadi. A three-dimensional cohesive-frictional grain-boundary micromechanical model for intergranular degradation and failure in polycrystalline materials. *Computer Methods in Applied Mechanics and Engineering*, 265:36–62, 2013.
- [5] I. Benedetti and F. Barbe. Modelling Polycrystalline Materials: An Overview of Three-Dimensional Grain-Scale Mechanical Models. *Journal of Multiscale Modelling*, 5:1–51, 2013.

- [6] B. Flipon, L. Garcia de la Cruz, E. Hug, C. Keller, and F. Barbe. Elaboration of austenitic stainless steel with bimodal grain size distribution and investigation of their mechanical behavior. AIP Conference Proceedings 1896, 200007, 20th Int. ESAFORM Conf. on Material Forming – ESAFORM 2017, 26-28 April 2017, Dublin, Ireland, 2017.
- [7] B. Flipon, C. Keller, and F. Barbe. Influence of bimodal microstructure morphologies on local and macroscopic mechanical responses. ECCOMAS Thematic Conference: Computational Modeling of Complex Materials across the Scales, CMCS 2017, 7-9 nov. 2017, Paris, France, 2017.
- [8] R. Guerchais, C. Robert, F. Morel, and N. Saintier. Micromechanical study of the loading path effect in high cycle fatigue. *International Journal of Fatigue*, 59:64–75, 2014.
- [9] A. Jean, F. Willot, S. Cantournet, S. Forest, and D. Jeulin. Large scale computations of effective elastic properties of rubber with carbon black fillers. *International Journal of Computational Multiscale Engineering*, 9:271–303, 2011.
- [10] D. Jeulin. Random tessellations and boolean random functions. In C. L. L. Hendriks, G. Borgefors, and R. Strand, editors, *Mathematical Morphology and Its Applications to Signal and Image Processing*, pages 25–36, Berlin, Heidelberg, 2013. Springer Berlin Heidelberg.
- [11] T. Kanit, F. N’Guyen, S. Forest, D. Jeulin, M. Reed, and S. Singleton. Apparent and effective physical properties of heterogeneous materials: representativity of samples of two materials from food industry. *Computer Methods in Applied Mechanics and Engineering*, 195:3960–3982, 2006.
- [12] C. Lautensack and T. Sych. 3D image analysis of open foams using random tessellations. *Image Analysis and Stereology*, 25:87–93, 2006.
- [13] C. Lautensack and S. Zuyev. Random Laguerre tessellations. *Advances in Applied Probability*, 40:630–650, 2008.
- [14] C. Morfa, M. de Farias, I. de Morales, E. de Navarra, and R. Valera. Virtual modeling of polycrystalline structures of materials using particle packing algorithms and Laguerre cells. *Computational Particle Mechanics*, 2017.
- [15] C. N’Guyen, F. Barbe, N. Osipov, G. Cailletaud, B. Marini, and C. Petry. Micromechanical local approach to brittle failure in bainite high resolution polycrystals: A short presentation. *Computational Materials Science*, 64:62–65, 2012.
- [16] C. Peyraga and D. Jeulin. Estimation of tortuosity and reconstruction of geodesic paths in 3D. *Image Analysis and Stereology*, 32:27–43, 2013.
- [17] R. Quey. Neper: polycrystal generation and meshing (version 3.1). <http://neper.sourceforge.net>, 2018.
- [18] R. Quey, P. Dawson, and F. Barbe. Large-scale 3-D random polycrystals for the finite element method: Generation, meshing and remeshing. *Computer Methods in Applied Mechanics and Engineering*, 200:1729–1745, 2011.
- [19] R. Quey and L. Renversade. Optimal polyhedral description of 3D polycrystals: method and application to statistical and synchrotron X-ray diffraction data. *Computer Methods in Applied Mechanics and Engineering*, 330:308–333, 2018.
- [20] C. Shao, P. Zhang, Y. Zhu, Z. Zhang, J. Pang, and Z. Zhang. Improvement of low-cycle fatigue resistance in TWIP steel by regulating the grain size and distribution. *Acta Materialia*, 134:128–142, 2017.
- [21] M. Sledzinska, B. Graczykowski, M. Placidi, D. Saleta Reig, A. El Sachat, J. Reparaz, F. Alzina, B. Mortazavi, R. Quey, L. Colombo, S. Roche, and C. Sotomayor Torres. Thermal conductivity of MoS<sub>2</sub> polycrystalline nanomembranes. *2D Materials*, 2016.
- [22] M. Sledzinska, R. Quey, B. Mortazavi, B. Graczykowski, M. Placidi, D. Saleta Reig, D. Navarro Urrios, F. Alzina, L. Colombo, S. Roche, and C. Sotomayor Torres. Record Low Thermal Conductivity of Polycrystalline MoS<sub>2</sub> films: Tuning the Thermal Conductivity by Grain Orientation. *ACS Applied Materials and Interfaces*, 9:37905–37911, 2017.
- [23] A. Zeghadi, S. Forest, A. Gourgues, and O. Bouaziz. Ensemble averaging stress-strain fields in polycrystalline aggregates with a constrained surface microstructure - Part 2: crystal plasticity. *Philosophical Magazine A*, 87:1425–1446, 2007.